Journal of Global Positioning Systems (2003)
Vol. 2, No. 1: 18-26

Journal of Global Positioning Systems
2003
© CPGPS

Dual-space Ambiguity Resolution Approach Theory and Application

Guorong Yu and Jingnan Liu

GPS Engineering Research Center, Wuhan University

Received: 23/10/2003 / Accepted: 12/11/2003

Abstract. In real time kinematic (RTK) GPS positioning the reference station(s) is (are) static, and the moving receivers must not be far from the reference station(s). But in some cases, such as formation flying, satellite-to-satellite orbit determination, etc, it is difficult to establish a static reference station. GPS kinematic-to-kinematic positioning (KINRTK) will meet such requirements. The key work of ambiguity resolution for KINRTK is to obtain an ambiguity float solution rapidly. The float solution can be estimated using either the "Geometry-based"(GB) or "Geometry-free"(GF) approach, requiring the construction of a "GB" or "GF" ambiguity search space. These two spaces are different but have the same true integer ambiguity result. Searching in two spaces at the same time, referred to here as Dual-space Ambiguity Resolution Approach (DARA), will be faster than in the individual spaces because only a few ambiguity candidates meet the conditions of both spaces simultaneously. It can be shown that DARA can dramatically reduce ambiguity candidates even if the C/A-code pseudo-range observables are used. The results of a vehicle test confirm that our approach is promising, resulting in millimeter-level misclosure of the KINRTK run.

Key words: GPS, Ambiguity Resolution, RTK

1 Introduction

On-the-fly GPS positioning relative to a moving reference, referred to as KINRTK in this paper, has many applications, such as formation flying, satellite-to-satellite orbit determination, and others, where a static reference is difficult to establish (e.g., Hermann et al., 1995, Kawano et al., 2001]. Quick integer carrier phase ambiguity estimation plays an important role in KINRTK. Once the ambiguities are resolved, centimeter-level accuracy of KINRTK can be achieved (e.g., Hermann et al., 1995).

In the GPS literature there are two of the many different approaches proposed for integer ambiguity estimation, which have drawn much interest. The two approaches differ in the model used for integer ambiguity estimation. In the first approach, which is the common mode of operation for most surveying applications, an explicit use is made of the available relative receiver-satellite geometry (e.g., Chen & Lachapelle, 1995, Frei & Butler, 1990, Teunissen, 1995) named the "GB"(GB) model by Teunissen (e.g., Teunissen, 1997). Integer ambiguity estimation is also possible however, when one opts for dispensing with the relative receiver-satellite geometry (e.g., Euler et al., 1991, Hatch, 1982, Horemuž, et al., 2002, Sjöberg, 1998), and is named the "GF"(GF) model. In fact from the conceptual point of view, this is the simplest approach to integer ambiguity estimation. The pseudo-range data are directly used to determine the unknown integer ambiguities of the observed phase data (e.g., Teunissen, 1997). These two models have their advantages and disadvantages. Combining their advantages this paper proposes an ambiguity resolution algorithm based on the integration of both ambiguity resolution approaches.

In our discussion below we assume that dual-frequency pseudo-range and carrier phase observables are available. In this paper the unit matrix of order p is denoted as $\boldsymbol{E}_p$ and the p-vector having all ones as entries is denoted as $\boldsymbol{e}_p$. Furthermore the canonical unit vector having the one as its i th entry is denoted as $\boldsymbol{c}_i$. 'vec' is the operator that transforms a matrix into a vector by stacking the columns of the matrix one underneath the other. The symbol '$\otimes$' denotes the Kronecker product (Teunissen, 1997):

$$\mathbf{A}\otimes\mathbf{B}=\begin{bmatrix} a_{11}\mathbf{B} & \cdots & a_{in}\mathbf{B} \\ \vdots & & \vdots \\ a_{n1}\mathbf{B} & \cdots & a_{nn}\mathbf{B} \end{bmatrix} \tag{1}$$

2 Observation Model

2.1 Satellite Geometry-based Model

Let us assume that double-differenced phase and pseudo-range observables are available. For each observed satellite (except for the one selected as the reference satellite), four observation equations can be written:

$$\begin{cases} R^{L1}=\rho+I+\delta R^{L1} \\ R^{L2}=\rho+r_{12}^2 I+\delta R^{L2} \\ \lambda^{L1}\phi^{L1}=\rho-I+\lambda^{L1}a^{L1}+\delta\phi^{L1} \\ \lambda^{L2}\phi^{L2}=\rho-r_{12}^2 I+\lambda^{L2}a^{L2}+\delta\phi^{L2} \end{cases} \tag{2}$$

where R^{L1}, R^{L2}, ϕ^{L1}, and ϕ^{L2} are phase and pseudo-range observables of the *L1* signal with wavelength λ^{L1} and frequency f^{L1}, and of the second signal *L2* with wavelength λ^{L2} and frequency f^{L2} respectively; ρ is the geometrical distance between receiver and satellite; a^{L1} and a^{L2} are integer ambiguities; I is the ionospheric errors of *L1* frequency; $r_{12}=f^{L1}/f^{L2}$; and δ are random observation errors. In the short baseline case, the ionospheric bias can be ignored (e.g., Kleusberg, 1986). The linearized observation equations at the i th epoch of m satellites are:

$$\mathbf{l}_i=\mathbf{B}_i\mathbf{b}_i+\left[\mathbf{E}_{m-1}\otimes\mathbf{A}\right]\mathbf{a}+\boldsymbol{\delta}_i \tag{3}$$

where $\mathbf{B}_i=\begin{bmatrix}\partial\rho\\ \partial b\end{bmatrix}$ $\mathbf{A}=\mathbf{c}_2\otimes\mathbf{E}_2$

$$\mathbf{l}_i=\left[R_1^{L1}\ \ R_1^{L2}\ \ \lambda^{L1}\phi_1^{L1}\ \ \lambda^{L2}\phi_1^{L2}\ \cdots R_{m-1}^{L1}\ \ R_{m-1}^{L2}\ \ \lambda^{L1}\phi_{m-1}^{L1}\ \ \lambda^{L2}\phi_{m-1}^{L2}\right]^{\mathrm{T}} \tag{4}$$

$$\mathbf{a}=\left[\lambda^{L1}a_1^{L1}\ \ \lambda^{L2}a_1^{L2}\ \ \cdots\ \ \lambda^{L1}a_{m-1}^{L1}\ \ \lambda^{L2}a_{m-1}^{L2}\right]^{\mathrm{T}} \tag{5}$$

$\boldsymbol{b}_i$ denotes the baseline vector of epoch i. The geometry of the double-differenced (DD) relative receiver-satellite configuration is contained within the (m-1)x3 matrix $\boldsymbol{B}_i$. It is well known that due to the high altitude orbits of the GPS satellites, the receiver-satellite geometry changes only slowly with time. The matrix $\boldsymbol{B}_i$ is therefore only weakly dependent on time. In our further analysis it will therefore be assumed that $\boldsymbol{B}_i$ is a time-invariant matrix, $\boldsymbol{B}_i=\boldsymbol{B}$. The k epochs linear system of DD observation equations are:

$$vec\mathbf{L}=(\mathbf{E}_k\otimes\mathbf{B})vec\mathbf{b}+\left[\mathbf{e}_k\otimes(\mathbf{E}_{m-1}\otimes\mathbf{A})\right]\mathbf{a}+\boldsymbol{\delta} \tag{6}$$

where

$$\mathbf{L}=\left[\mathbf{l}_1\ \ \mathbf{l}_2\ \ \cdots\ \ \mathbf{l}_k\right]\quad\mathbf{b}=\left[\mathbf{b}_1\ \ \mathbf{b}_2\ \ \cdots\ \ \mathbf{b}_k\right]$$

2.2 Satellite Geometry-free Model

In this model the observation equations are not parametrized in terms of the baseline components. Instead, they remain parametrized in terms of the unknown DD receiver-satellite ranges. This implies that the observation equations remain linear and that the receiver-satellite geometry is not explicitly present in these equations. Hence the model permits both receivers to be either stationary or moving.

$$\mathbf{l}_i=\left[\mathbf{E}_{m-1}\otimes\mathbf{e}_4\right]\boldsymbol{\rho}^i+\left[\mathbf{E}_{m-1}\otimes\mathbf{A}\right]\mathbf{a}+\boldsymbol{\delta}_i \tag{7}$$

where $\boldsymbol{\rho}^i=\left[\rho_1\ \ \rho_2\ \ \cdots\ \ \rho_{m-1}\right]^{\mathrm{T}}$. The k epochs system of DD observation equations are:

$$\begin{aligned} vec\mathbf{L}=&\left[\mathbf{E}_k\otimes(\mathbf{E}_{m-1}\otimes\mathbf{e}_4)\right]vec\boldsymbol{\rho}\\ &+\left[\mathbf{e}_k\otimes(\mathbf{E}_{m-1}\otimes\mathbf{A})\right]\mathbf{a}+\boldsymbol{\delta}\end{aligned} \tag{8}$$

where $\boldsymbol{\rho}=\left[\boldsymbol{\rho}^1\ \ \boldsymbol{\rho}^2\ \ \cdots\ \ \boldsymbol{\rho}^k\right]$. For further details we refer readers to Teunissen (e.g., Teunissen, 1997).

3 Shape and Orientation of Ambiguity Search Space

In our analysis we assume that the variance matrix of the observables is given by: $\boldsymbol{\Sigma}=\boldsymbol{E}_k\otimes\boldsymbol{P}$. Solved by the least squares adjustment method, the normal equations are:

$$\mathbf{N}\mathbf{X}=\mathbf{U} \tag{9}$$

$$\mathbf{N}=\begin{bmatrix}\mathbf{E}_k\otimes\mathbf{B}^{\mathrm{T}}\mathbf{P}\mathbf{B} & \mathbf{e}_k\otimes\mathbf{B}^{\mathrm{T}}\mathbf{P}\mathbf{A}\\ \mathbf{e}_k^{\mathrm{T}}\otimes\mathbf{A}^{\mathrm{T}}\mathbf{P}\mathbf{B} & \sum\mathbf{A}^{\mathrm{T}}\mathbf{P}\mathbf{A}\end{bmatrix}=\begin{bmatrix}\mathbf{N}_{11} & \mathbf{N}_{12}\\ \mathbf{N}_{21} & \mathbf{N}_{22}\end{bmatrix} \tag{10}$$

$$\mathbf{U} = \begin{bmatrix} \mathbf{E}_k \otimes (\mathbf{B}^{\mathrm{T}}\mathbf{P}) \\ \mathbf{e}_k^T \otimes (\mathbf{A}^{\mathrm{T}}\mathbf{P}) \end{bmatrix} vec\mathbf{L} \tag{11}$$

and the variance of the ambiguities is:

$$\mathbf{Q}_{aa} = (N_{22} - N_{21}N_{11}^{-1}N_{12})^{-1} = (\Sigma\mathbf{Q}_i)^{-1}, \quad \mathbf{U}_a = (\Sigma\mathbf{U}_i) \tag{12}$$

$$\mathbf{Q}_i = \mathbf{A}^{\mathrm{T}}\mathbf{P}_i\mathbf{A} - \mathbf{A}^{\mathrm{T}}\mathbf{P}_i\mathbf{B}_i(\mathbf{B}_i^{\mathrm{T}}\mathbf{P}_i\mathbf{B}_i)^{-1}\mathbf{B}_i^{\mathrm{T}}\mathbf{P}_i\mathbf{A} \tag{13}$$

$$\mathbf{U}_i = \mathbf{A}^{\mathrm{T}}\mathbf{P}_i\mathbf{l}_i - \mathbf{A}^{\mathrm{T}}\mathbf{P}_i\mathbf{B}_i(\mathbf{B}_i^{\mathrm{T}}\mathbf{P}_i\mathbf{B}_i)^{-1}\mathbf{B}_i^{\mathrm{T}}\mathbf{P}_i\mathbf{l}_i \tag{14}$$

where the subscript index i means the epoch i. The matrix $\boldsymbol{B}_i$ of the GB model is the linearized matrix of equation (1), while $\boldsymbol{B}_i$ of the GF model is $\boldsymbol{B}_i = \boldsymbol{E}_{m-1} \otimes \boldsymbol{e}_4$. Assume σ_{L1}=0.0019m, σ_{L2}=0.0024m, σ_{CA}=3.0m, σ_{P2}=0.3m, and selecting 5 satellites and 50 epochs of kinematic observables, we get the variance-covariances of the ambiguities of the GB model:

$$\boldsymbol{Q}_{aa} = \begin{bmatrix} 0.15 & 0.12 & 0.07 & 0.06 & 0.09 & 0.07 & 0.07 & 0.06 \\ & 0.09 & 0.06 & 0.04 & 0.07 & 0.05 & 0.06 & 0.04 \\ & & 0.18 & 0.14 & 0.09 & 0.07 & 0.09 & 0.07 \\ & & & 0.11 & 0.07 & 0.05 & 0.07 & 0.05 \\ & & & & 0.13 & 0.10 & 0.14 & 0.11 \\ & & & & & 0.08 & 0.11 & 0.08 \\ & SYS & & & & & 0.15 & 0.12 \\ & & & & & & & 0.09 \end{bmatrix} \tag{15}$$

The variance-covariances of the ambiguities for the GF model are:

$$\boldsymbol{Q}_{aa} = \begin{bmatrix} 0.20 & 0.15 & 0.10 & 0.08 & 0.10 & 0.08 & 0.10 & 0.08 \\ & 0.12 & 0.08 & 0.06 & 0.08 & 0.06 & 0.08 & 0.06 \\ & & 0.20 & 0.15 & 0.10 & 0.08 & 0.10 & 0.08 \\ & & & 0.12 & 0.08 & 0.06 & 0.08 & 0.06 \\ & & & & 0.20 & 0.15 & 0.10 & 0.08 \\ & & & & & 0.12 & 0.08 & 0.06 \\ & SYS & & & & & 0.20 & 0.15 \\ & & & & & & & 0.12 \end{bmatrix} \tag{16}$$

Of particular interest here is the shape and orientation of the ellipsoid of standard deviation for the ambiguities (e.g., Leick, 1995). The semi-minor and semi-major axes and the orientation are given in Tab. 1 to 8.

Tab 1 Semi-major axes for the GB model (m)

		1	2		3		4	
		L2	L1	L2	L1	L2	L1	L2
1	L1	0.49	0.49	0.43	0.48	0.44	0.47	0.43
	L2		0.45	0.38	0.43	0.37	0.43	0.37
2	L1			0.54	0.49	0.46	0.51	0.47
	L2				0.43	0.39	0.45	0.40
3	L1					0.46	0.53	0.47
	L2						0.48	0.41
4	L1							0.50

Tab 2 Semi-minor axes for the GB model (m)

		1	2		3		4	
		L2	L1	L2	L1	L2	L1	L2
1	L1	**0.003**	0.30	0.265	0.22	0.189	0.28	0.239
	L2		0.25	0.236	0.19	0.173	0.24	0.217
2	L1			**0.003**	0.26	0.216	0.27	0.232
	L2				0.23	0.202	0.24	0.214
3	L1					**0.003**	0.05	0.046
	L2						0.05	0.041
4	L1							**0.003**

Tab 3 Semi-major axes for the GF model (m)

		1	2		3		4	
		L2	L1	L2	L1	L2	L1	L2
1	L1	0.56	0.54	0.49	0.54	0.49	0.54	0.49
	L2		0.49	0.42	0.49	0.42	0.49	0.42
2	L1			0.56	0.54	0.49	0.54	0.49
	L2				0.49	0.42	0.49	0.42
3	L1					0.56	0.54	0.49
	L2						0.49	0.42
4	L1							0.56

Tab 4 Semi-minor axes for the GF model (m)

		1	2		3		4	
		L2	L1	L2	L1	L2	L1	L2
1	L1	**0.003**	0.31	0.269	0.31	0.269	0.31	0.269
	L2		0.27	0.244	0.27	0.244	0.27	0.244
2	L1			**0.003**	0.31	0.269	0.31	0.269
	L2				0.27	0.244	0.27	0.244
3	L1					**0.003**	0.31	0.269
	L2						0.27	0.244
4	L1							**0.003**

Tab 5 The orientation for the GB model (Degree)

		1	2		3		4	
		L2	L1	L2	L1	L2	L1	L2
1	L1	**37.93**	51.27	35.26	42.27	31.97	45.78	31.93
	L2		64.54	51.27	53.14	42.27	59.33	45.78
2	L1			**37.93**	37.00	26.45	40.64	29.02
	L2				49.68	37.00	53.54	40.64
3	L1					**37.93**	47.19	39.93
	L2						54.30	47.19
4	L1							**37.93**

Tab 6 The orientation for the GF model (Degree)

		1	2		3		4	
		L2	L1	L2	L1	L2	L1	L2
1	L1	**37.93**	45.00	31.62	45.00	31.62	45.00	31.62
	L2		58.38	45.00	58.38	45.00	58.38	45.00
2	L1			**37.93**	45.00	31.62	45.00	31.62
	L2				58.38	45.00	58.38	45.00
3	L1					**37.93**	45.00	31.62
	L2						58.38	45.00
4	L1							**37.93**

Tab 7 The orientation for the GB model with 100 epochs (Degree)

		1	2		3		4	
		L2	L1	L2	L1	L2	L1	L2
1	L1	**37.93**	66.42	47.21	50.92	39.25	58.31	44.00
	L2		75.71	66.42	61.22	50.92	68.46	58.31
2	L1			**37.93**	36.84	25.46	42.81	30.19
	L2				50.87	36.84	56.17	42.81
3	L1					**37.93**	48.09	40.86
	L2						55.11	48.09
4	L1							**37.93**

Tab 8 The orientation for the GB model with 150 epochs (Degree)

		1	2		3		4	
		L2	L1	L2	L1	L2	L1	L2
1	L1	**37.93**	80.11	69.80	59.00	47.67	66.90	55.73
	L2		83.82	80.11	67.55	59.00	73.87	66.90
2	L1			**37.93**	36.68	24.61	44.43	31.02
	L2				51.91	36.68	58.04	44.43
3	L1					**37.93**	48.66	41.46
	L2						55.63	48.66
4	L1							**37.93**

The orientation for the GF model does not change as the number of epochs increases. The orientation of L1 and L2 for the same satellite is exactly $37.93°$, i.e., the slope is $k = \lambda_1 / \lambda_2$, and the semi-minor axes for the GB are equal to those of the GF model, while the semi-major axes for the GF model are longer than those of the GB model, which means that the ellipse for the GF model always contains the ellipse for the GB model (see Fig.1). The geometry is the same for every epoch solution, as long as the stochastic model remains unchanged.

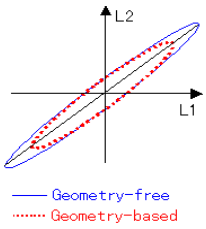

Fig.1 The ellipse of L1-L2

The orientation for the GF model does not change for every epoch, while the orientation of two different satellites for the GB model is closer to the axes as the number of epochs increases, which means that these two ellipses overlap each other partly (see Fig.2).

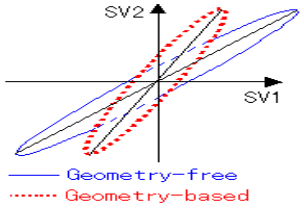

Fig. 2 The ellipse of SV1-SV2

As can been seen from Tab. 1 to 8 and Fig.1, the ellipse of L1-L2 is almost a straight line with a slope of $k = \lambda_1 / \lambda_2$. If (a^{L1}, a^{L2}) is the nearest point to the line, the next nearest points are $(a^{L1} \pm 9, a^{L2} \pm 7)$, which means if (a^{L1}, a^{L2}) is an ambiguity candidate, the next candidates are exactly $(a^{L1} \pm 9, a^{L2} \pm 7)$. Because the semi-minor axes are very short, the ellipse nearly only contains points such as $(a^{L1} \pm \text{k*9}, a^{L2} \pm \text{k*7})$, k=0,1,2… Therefore, the key task for ambiguity resolution is to obtain the float ambiguity solution.

4 Linear Combination of Two Frequency Observations

Let's consider a linear transformation (e.g., Han & Rizos, 1996, Teunissen, 1995):

$$\phi_{m,n} = m\phi^{L1} + n\phi^{L2} \tag{17}$$

If we set (m, n) = (-7,9), all points like $(a^{L1} \pm \text{k*9}, a^{L2} \pm \text{k*7})$, k=0,1,2…will be mapped to one point (a^{L1}, a^{L2}). In other words, the semi-major axes (or the ellipse because of very short semi-minor axis) is mapped to a point (see Fig.1). But if the integer solution $\breve{a}_{m,n}$ has been obtained, the solution $(\breve{a}^{L1}, \breve{a}^{L2})$ can not be determined by an inverted transform. So let's consider another linear transform:

$$\phi_{i,j} = i\phi^{L1} + j\phi^{L2} \tag{18}$$

As $(a^{L1} \pm 5, a^{L2} \pm 4)$ are the next points near to the semi-major axes, we choose (i, j) = (+4,-5). Using these two transforms at the same time:

$$\begin{bmatrix} \phi_{i,j} \\ \phi_{m,n} \end{bmatrix} = \begin{bmatrix} i & j \\ m & n \end{bmatrix} \begin{bmatrix} \phi^{L1} \\ \phi^{L2} \end{bmatrix} = \mathbf{H} \begin{bmatrix} \phi^{L1} \\ \phi^{L2} \end{bmatrix} \tag{19}$$

the ambiguities are:

$$\begin{bmatrix} a_{i,j} \\ a_{m,n} \end{bmatrix} = \mathbf{H} \begin{bmatrix} a^{L1} \\ a^{L2} \end{bmatrix} \tag{20}$$

Fig.3 shows the single epoch DD ambiguity float solution for satellites 31 to 11 of rover1 versus rover2 (refer to Fig.8) processed using the GB model. The horizontal axis is GPS Seconds of Week (GSW), the vertical axis is the float solution, and "0" is the integer ambiguity solution. Fig.4 shows the single epoch ambiguity float solution processed using the GF model. From Fig.3 and Fig.4, we can see that the float solution undulates around the fixed

solution.

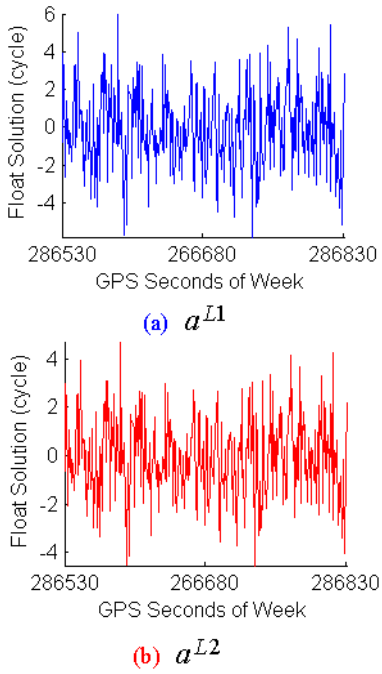

Fig.3 Single epoch ambiguity float solution processed by the GB model

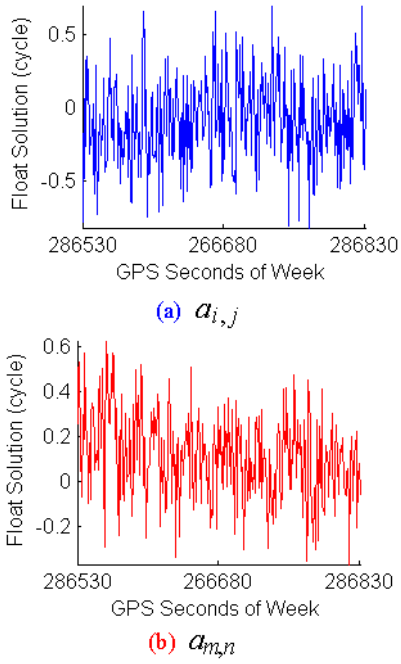

Fig.4 Single epoch ambiguity float solution processed by the GF model

5 Ambiguity Search Strategy

Let us assume that the observables $\phi^{L1}, \phi^{L2}, R^{CA}, R^{P2}$ are not correlated, and that the standard errors of the observables are σ_{L1}=0.0019m, σ_{L2}=0.0024m, σ_{CA}=3.0m, σ_{P2}=0.3m, then the standard errors of the linear combination ambiguities are $\sigma_{a_{i,j}}$=0.35, $\sigma_{a_{m,n}}$=0.23 with (i, j) = (+4,-5) and (m, n) = (-7,9), and the ratio of semi-major axis to semi-minor axis is 35:22, which means that the area of the search ellipse is almost equal to that of the confidence interval determined by $(\hat{a} \pm k * \sigma_{\hat{a}})$, see Fig.5.

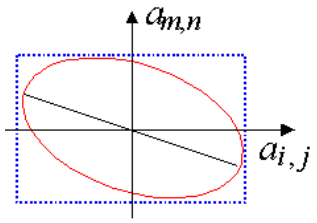

Fig. 5 Difference between the confidence ellipse and the confidence interval of the ambiguity parameters

We obtain the ambiguity search space of the GF model (GF) by estimating $a_{i,j}$ and $a_{m,n}$. On the other hand, we can construct the ambiguity search space of the GB model (GB) by processing the original observables ϕ^{L1}, ϕ^{L2}. When the $a_{i,j}$ and $a_{m,n}$ are fixed, a^{L1} and a^{L2} can be determined from equation (20), and vice versa. But other candidates may not keep the map relation, i.e. if we map a candidate of GB using equation (20), it would not belong to GF, and vice versa, due to these two spaces being constructed using two different models. Assume the GF is $(a_{i,j}, a_{m,n}) \in$ F, F= $(\hat{a} \pm k * \sigma_{\hat{a}})$, k=4; and GB is $(a^{L1}, a^{L2}) \in$ B, B=[-10,10]×[-10,10], i.e. 441 candidates. Then we get Tab. 9.

Tab 9 The relationship between GF and GB

$a_{i,j}$	-1	0	-1	**0**	1	0	1
$a_{m,n}$	1	-1	0	**0**	0	1	-1
a^{L1}	-4	-5	-9	**0**	9	5	4
a^{L2}	-3	-4	-7	**0**	7	4	3
$\|\Delta\|$	0.15	0.13	0.02	**0.00**	0.02	0.13	0.15

In Tab.9, $|\Delta|$ is the distance of an ambiguity candidate (a^{L1}, a^{L2}) to the semi-major axis. For example:

Assume the integer ambiguity solution is:

$(\breve{a}^{L1}, \breve{a}^{L2})$=(-2035428, -1583755)
and the float solution processed by the GF model is:

$(\hat{a}_{i,j}, \hat{a}_{m,n})$=(-226937.146, 1201.609)

whose nearest integers are:

(-226937, 1202)

the candidates within the confidence interval F= $(\hat{a} \pm k * \sigma_{\hat{a}})$, k=4 become:

(-226937 ± 1, 1202), (-226937, 1202), (-226937 ± 1, 1201), (-226937, 1201)

While the float solution processed by the GB model is:

$(\hat{a}^{L1}, \hat{a}^{L2})$=(-2036430.867, -1583757.208)

whose nearest integers are:

(-2036431, -1583757)

and assuming the confidence intervals are:

(-2036431 ± k, -1583757 ± k), k=-10,-9… -1,0,+1,…,+9,+10

then the candidates selected by Tab. 9 become:

(-2036428+5-9, -1583755+4-7), (-2036428+5, -1583755+4), (-2036428-9, -1583755-7), (-2036428, -1583755)

Only four candidates need to be considered further, see Fig. 6.

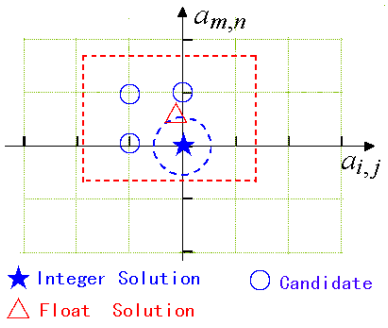

Fig. 6 Ambiguity candidates

Tab. 9 also means that ambiguities a^{L1} and a^{L2} or $a_{i,j}$ and $a_{m,n}$ should be searched in pairs in one loop, not two individual loops! In other words, if there are five satellites, eight double-differenced observables are formed, and the number of ambiguity search loops is four, not eight.

The next step is to consider the search ellipses of different satellites. The selected candidate which is processed by the GF model should be located in the search ellipse of the GB model. In other words, the distance of the candidate to the semi-major axis of the search ellipse of the GB should be not longer than the length of the semi-minor axis of the search ellipse, see Fig.7.

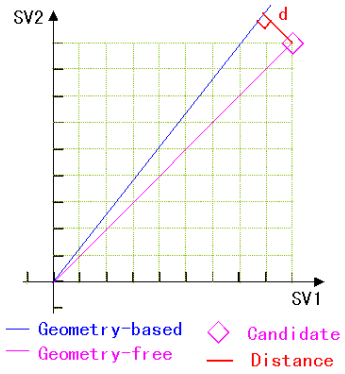

Fig. 7 The distance of the candidate to the semi-major axis.

6 Test and Results

6.1 Vehicle Test

A vehicle kinematic test was performed (see Fig.8). The following are details of the experiment:

Site: MingZu Road, Wuhan City, China
Time: 19-12-2001, 15:00-16:30 (Local time);
Receivers: Three Trimble 4700;
Sample: 1 second; and
Elevation: 15 degree.

One receiver was set as a static reference (named "base station"), the other two were mounted on two vehicles, (named "rover1" and "rover2"). First, 30 minutes of static observations were collected by the three receivers. Then rover1 moved fast and rover2 followed. 20 minutes later these two receivers stopped moving and a five-minute period of static observations were collected. Then back to the starting place, and another five minutes of static observations were again collected.

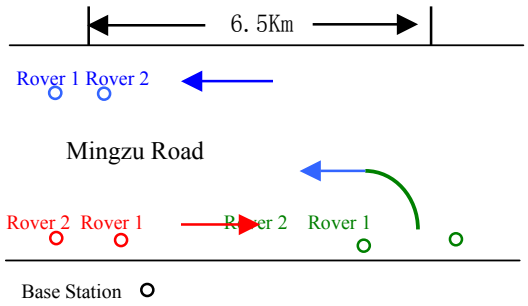

Fig.8 Kinematic test scenario

6.2 Ambiguity Resolution

The kinematic test data were processed by the proposed DARA (Dual-space Ambiguity Resolution Approach) method, i.e., searching ambiguities in two spaces at the same time, also using a least squares (LS) ambiguity search approach, i.e., searching ambiguities only in the GB ambiguity space (and validating by the "Ratio" test). Tab. 10 is a summary of the ambiguity resolution results.

Tab 10 Summary of ambiguity resolution results

Baseline	Epochs	LS			DARA		
		True	Wrong	Success Rate	True	Wrong	Success Rate
Rover2 -Rover1	5	885	132	0.87	989	28	0.97
	10	440	68	0.86	501	7	0.99
Base -Rover1	5	909	108	0.89	1007	10	0.99
	10	456	52	0.89	502	6	0.99
Base -Rover2	5	915	102	0.89	993	24	0.97
	10	461	47	0.90	501	7	0.99

6.3 Positioning

Fig.9 (a) shows the "static-kinematic" results, the solid line is rover1 to base station and the dotted line is rover2. Fig.9 (b) shows the "kinematic-kinematic" results, i.e. rover2 is a moving reference. As we can see, the three receivers started observing at 284530 GSW, rover1 and rover2 began moving at 286930 GSW, relative static (not static) at 287870 GSW, then back at 288230, then relative static at 289260, and the test was stopped at 289618 GSW.

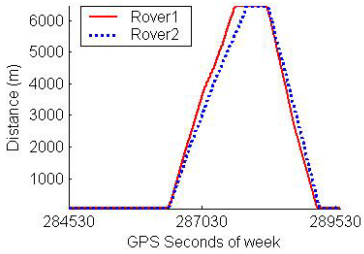

(a)

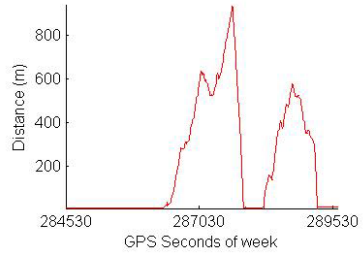

(b)

Fig.9 Distances between receivers

Fig.10 (a) shows the comparison of static-kinematic to kinematic-kinematic. The solid line is the distance between rover2 and rover1, while the dotted line is calculated from the two static-kinematic baselines, i.e. base station-rover1 and base station-rover2. Fig.10 (b) shows the difference between the two lines of Fig.16 (a).

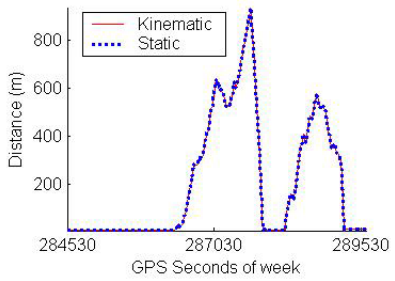

(a)

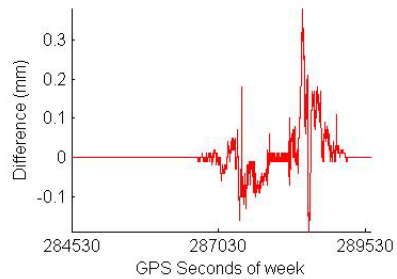

(b)

Fig.10 A Comparison of static and kinematic results

Fig.11 shows the misclosure of the three baselines. The results show that millimeter-level misclosure was achieved.

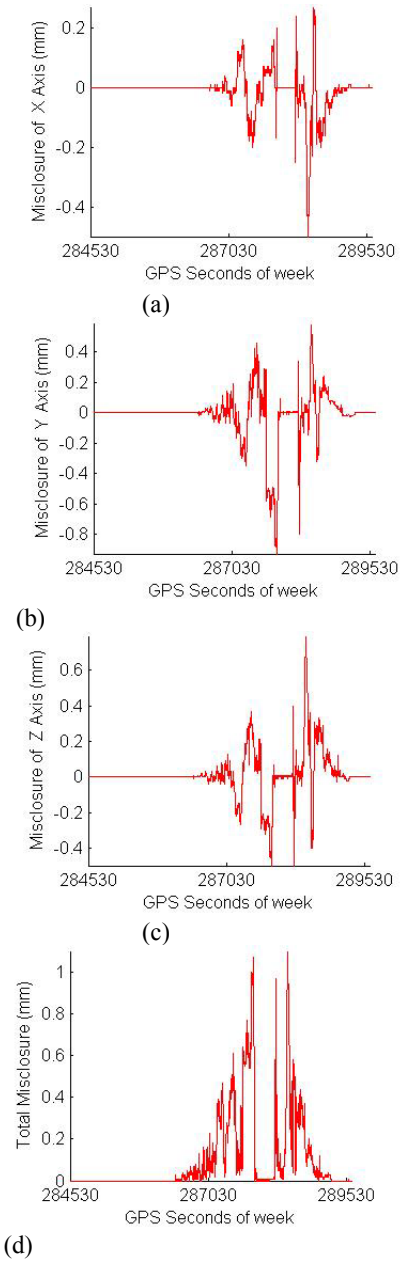

Fig.11 Misclosure of the three baselines

7 Conclusion

Carrier phase ambiguity resolution is the key to fast and high precision GPS parameter estimation. The float solution can be estimated by two kinds of models which may have the relative receiver-satellite geometry included (GB) or excluded (GF), and used to construct "GB" or "GF" ambiguity search spaces. These two models have their advantages and disadvantages. Further analysis shows these two spaces are different but have the same true ambiguity resolution result. A new concept for ambiguity resolution, called Dual-space Ambiguity Resolution Approach (DARA), involving a search in both spaces at the same time, is proposed. In this paper the vehicle test shows that the DARA performed well, resulting in millimeter-level misclosure.

Acknowledgments

We are grateful to Prof. Chris Rizos for useful comments and for his help in the English expression. We also like to thank Dr. Liu Xianglin for his reviews of this paper.

References

Hermann, B.R., Evans. A.G., Law. C.S., *et al*. (1995). ***Kinematic on the fly GPS Positioning Relative to a Moving reference***. NAVIGATION: Journal of the Institute of Navigation, 42(3): 487-501.

Kawano, I., Mokuno, M., Kasai, T., *et al*. (2001) ***First Autonomous Rendezvous Using Relative GPS Navigation By ETS_VII***. NAVIGATION: Journal of the Institute of Navigation, **48**(1): 49-56.

Chen, D., Lachepelle, G., (1995) ***A Comparison of The FASF and Least Squares Search Algorithms For On-The-Fly Ambiguity Resolution***. NAVIGATION: Journal of the Institute of Navigation, **42**(2): 371-390.

Frei, E., Beutler, G., (1990) ***Rapid Static Positioning Based On The Fast Ambiguity Resolution Approach "FARA":*** Theory and First Results. Manuscripta Geodaetica, **15**(6): 325-356.

Teunissen, P.J.G., (1995) ***The Least-squares Ambiguity Decorrelation Adjustment: A Method for GPS Integer Ambiguity Estimation.*** Journal of Geodesy. **70**(1-2): 65-82.

Teunissen, P.J.G., (1997) ***GPS Double Difference Statistics: With and Without Using Satellite Geometry*. Journal of Geodesy, 71**(3): 137-148.

Euler, H. J., and Goad, C.C., (1991) ***On Optimal Filtering of GPS Dual Frequency Observations Without Using Orbit Information***. Bull.Geod, 63(2): 130-143.

Hatch, R., (1982) ***The Synergism of GPS Code and Carrier Measurements***. In Proceedings of the Third International Geodetic Symposium on Satellite Doppler Positioning,MA, Las Cruces, New Mexico, 1213–1232.

Horemuž, M., and Sjöberg, L.E., (2002) ***Rapid GPS Ambiguity Resolution For Short And Long Baselines[J].*** Journal of Geodesy, **76**(6-7), 381-391.

Sjöberg, L.E.,(1998) ***A new method for GPS phase base ambiguity resolution by combined phase and code observables.*** Surv Review, **34**(268): 363-372.

Kleusberg, A., (1986). ***Ionospheric Propagation Effects In Geodetic Relative GPS Positioning.*** Manuscripta Geodaetica, Vol.11, No.4, 256-261.

Leick, A., (1995) ***GPS Satellite Surveying***, second edition John wiley & sons.inc. New York, 560pages.

Han, S., and Rizos, C., (1996) ***Improving the computational efficiency of the ambiguity function algorithm***. Journal of Geodesy, **70**(6): 330-341.

Teunissen, P.J.G., (1995) ***The invertible GPS ambiguity transformations.*** Manuscripta geodaetica, **20**(6): 489-497.